Dynamic Modeling of an Optimal Hybrid Power System for a Captive Power Plant in Pakistan

Luqman Ahsan[1*] iD, M. Tariq Iqbal[2] iD

[1, 2] Department of Electrical and Computer Engineering, Faculty of Engineering and Applied Science, Memorial University of Newfoundland, Newfoundland, Canada
E-mail: lahsan@mun.ca

Abstract — This paper presents the optimized design, economic feasibility and dynamic modeling of a grid-tied captive hybrid renewable energy power plant for a Pakistani industrial area. Since the proposed plant, encompasses a photovoltaic (PV) array - as its main component - and for an efficient and reliable operation many issues - including industrial load variations and expected dynamics - should be investigated before its implementation. In this context, Homer Pro software is utilized in the design and economic optimized sizing of the PV array, and the PVWatts is used in land requirement analysis. The designed grid-tied plant is modeled in the MATLAB/Simulink using Simscape blocksets to investigate the plant's dynamic behavior due to typical practical disturbances. The obtained results reveal that the plant has a low per-unit energy cost and provides significant savings. Results of dynamic simulation show that the plant can respond to the ramp-up and ramp-down load variations in industrial settings. Moreover, the plant has a fast response to step changes in irradiance; proving that the proposed plant is reliable and suitable candidate for fulfilling the designated load.

Keywords — Captive power plant; Hybrid renewable energy power system; Dynamic modeling; Optimized design; Economic feasibility; HOMER Pro; PVWATT software; Dynamic modeling.

1. INTRODUCTION

Electricity is one of the basic requirements for the survival of modern life. It plays a vital role in the sustainable economy of any country. According to the International Energy Agency (IEA), 992 million people did not have electricity in 2018 and that almost 674 million would remain without electricity by 2030 [1]. Different energy resources are converted into electricity using specific methods depending upon the type of fuel. As a result of electricity generation from fossil fuels, a large amount of CO_2 is being emitted, which harms the environment and causes global warming. In 2020, the National Aeronautics and Space Administration (NASA) estimated that global temperature rose by 1.02°C since 1880 [2]. Since depletion of fossil fuels is happening, it is inevitable to have a smooth shift to other abundant clean resources such as solar, wind, tidal, etc.

Renewable resources are non-consumables and give zero emission during use. For instance, a 1000 W photovoltaic (PV) system producing 150 kWh/month, impedes 75 kg of fossil being mined, ultimately stopping 150 kg of CO_2 from being injected into the environment [3]. Output energy from these resources depends on environmental factors such as irradiance, temperature, air, etc., which disturb the electric grid's stability and cause tripping.

For a country like Pakistan, solar energy is considered the most suitable renewable energy source. Due to the intermittency of solar energy, electricity is generated from systems that combine different energy resources like solar, coal, gas, furnace oil etc. Such systems are called hybrid power systems [4]. There are two basic types of hybrid energy systems: i) grid-

connected and ii) standalone. Standalone systems are suitable for remote locations where it is difficult to supply power, and the system operates in islanding mode. The standalone system requires batteries for sustainable operation during night time and stormy weather. Therefore, these systems have a low load factor (LF) which increases the capital and maintenance costs [5]. For the grid-connected systems, installation location should be near the main grid where they can be synchronized with the national grid. In this case, the grid acts as batteries and can deliver or absorb the extra power generated by the hybrid system.

Many studies have been done on hybrid renewable energy systems (HRES) to achieve a lower cost. In literature, various methods have been used to optimize PV systems and dynamic analysis. In order to size a PV system, two techniques are used. One is a computer-based method, and the other is manual formulation method [6]. Over time, many manual methods are eliminated due to the modern development in computer-aided tools. In the old methods, mathematical formulas mainly consider the tilt angle, irradiance, storage, etc., for sizing purposes. Four coefficients are required in the manual sizing method called loss of load probability to design the standalone PV system [7].

Computer-aided tools are used for accurate and perfect sizing because a computer can perform tedious calculations in a very short time and give more accurate results. In the utilized software, load profile and site selection are required, and it obtains the weather data from the assigned directory. There are many softwares for sizing and optimization of PV systems. For example, PV planner, system advisor model (SAM), PVsyst, HOMER, etc.

The authors of [8] developed a linear programming-based model for finding the ecological and economic optimized off-grid system. The model was tested on two different continent countries; one in India and the other in Columbia. It was found that sizing the optimized system depends mainly on the load demand of the site, and that the renewable system provides significant fuel saving. In [9], the authors studied the economic feasibility HRES for rural electrification in Iran, and discussed the penetration of renewable energy to fed current to the grid HOMER. Tahir et al. [10] designed a grid-tied HRES in which a diesel generator is used along with a PV system. A 3-kW power system is modeled, and optimization analysis is carried out using the HOMER Pro.

Nurunnabi et al. [11] designed a PV system for a rural area in Bangladesh with very low load demand of 60 kW, and small load fluctuation. Chaichan et al. [12] studied various design cases for a solar water pumping system in a rural site in Oman. The cost of energy was found to be US$ 0.4743/kWh which was cheapest and have 0 % carbon emissions. A system is designed for Bani Walid, Libya, which has an average load demand of 35.98 MW and peak load demand of 85 MW [13]. The financial optimization was done in HOMER and the results showed that 76.8 MW PV system along with 26 Hoppecke batteries are required to fulfill the load. A detail scenario of renewable energy policies in Indian state of Gujarat is discussed in [14], and some social barriers in the way of renewable energy and their solutions were identified. Benalcazar et al. [15] performed an optimized sizing and scheduling of hybrid energy system for Morona Santiago and the Galapagos Islands. A mathematical programming model was used for technical and economic feasibility of two islanding PV systems. The results showed that the hybrid system is suitable for eliminating the subservience of rural areas on fossil fuels and providing power to remote areas. In [16], the author designed and simulated a PV system for a boat carrying 20 passengers in

Bangladesh. From HOMER sizing results, 10.6 kW PV system is required. DC motors were used; therefore, no inverter is required for this system.

In [17], electrification of rural operate in the islanding mode of operation was investigated. PV was used to provide power during sunny days, and diesel/gas gensets were used as a backup for providing power during emergency conditions.

The above reviewed works indicate that a lot of work has been done on the sizing, optimization, and scheduling of systems for economic feasibility, but no significant study is available on the dynamics of a hybrid power system. The power system security, resilience, and stability are crucial for the consumer's reliable and uninterruptable power supply. In this regard, it is crucial, after sizing the PV system, to look deeper at the steady-state and transient behavior of grid-tied systems because the power system is always under disruptions due to continuous fluctuations in load and solar irradiance. Therefore, the system should be stable enough to bear such changes. Different software's are used for studying the dynamic modeling such as power factory Dig SILENT, LabVIEW, Matlab/Simulink, etc. But Simulink is considered one of the best softwares since it provides a broader view of the system response.

Many researchers have investigated the possibility of utilizing small PV systems for houses, water pumps, reverse osmosis plants, etc.; but no pertinent research is reported on using hybrid systems for fulfilling the load of industrial units on a utility scale with extensive load variations. In this regard, this paper proposes a HRES for meeting the load of an industrial complex, Shafi Texcel Limited located in Pakistan (31.2616, 74.1674). The average load of the industry is 2185 kW and the peak load is 3100 kW which has LF of 76%. The load data of the 2020 - used for system sizing purposes - is depicted in Fig. 1. The load fluctuations in Fig. 1 during April and May are due to the Covid-19 lockdown placed by the government.

The designed system should meet the following requirements:
- Provide lowest levelized cost of energy (LCOE).
- Respond to rapid changes in irradiance.
- Reduce the steady state error by implementing an integral regulating technique in incremental conductance (IC) method.
- Handle the abrupt change in consumer load because there are significant variations in industrial load.
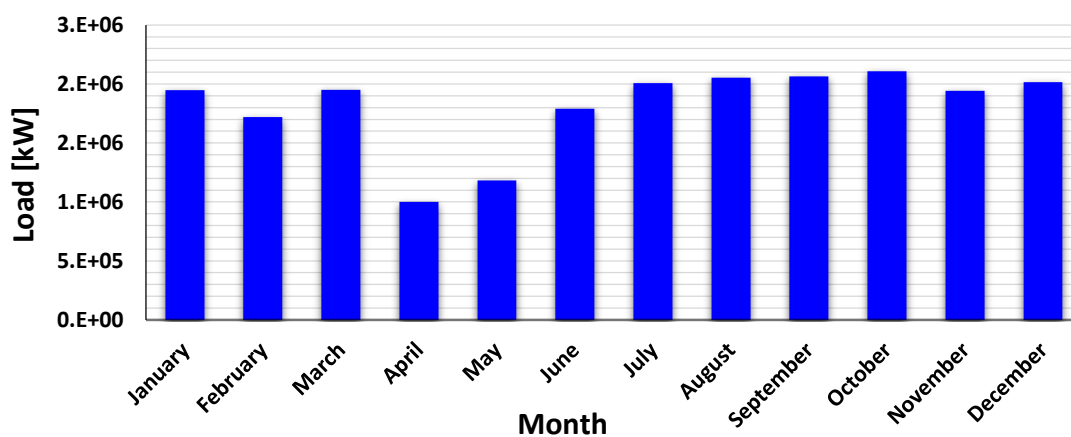

Fig. 1. Monthly load of the industrial complex.

2. MATHEMATICAL MODELING OF HRES

Mathematical modeling of the proposed HRES components is discussed in the following subsections.

2.1. PV Array Sizing

Schematic diagram of the proposed HRES is depicted in Fig. 2, and the detailed system design was reported in [18], and the system's land marking is exhibited in Fig. 3. The optimization results indicated that a 8382 kW$_{dc}$ capacity PV array is required for the selected site. To generate the desired input voltage, 13 modules of 480 W are connected in series and 670 such series modules are connected in parallel. There are two such strings to generate the required power.
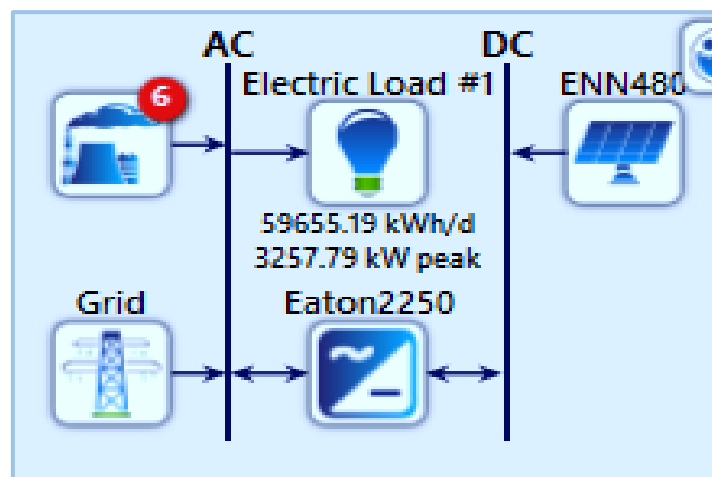
Fig. 2. Schematic diagram of the proposed HRES in HOMER Pro.

Fig. 3. Land marking of the proposed HRES.

The 480W PV module specifications are given in Table 1. Fig. 4 shows the current-voltage (I-V) and power-voltage (P-V) characteristics of the utilized PV array. It reveals that the maximum power point voltage of one string is 679 V at 25 °C and maximum power point current is 6190.8 A.

Table 1. Specifications of the 480 W HELIENE PV module.

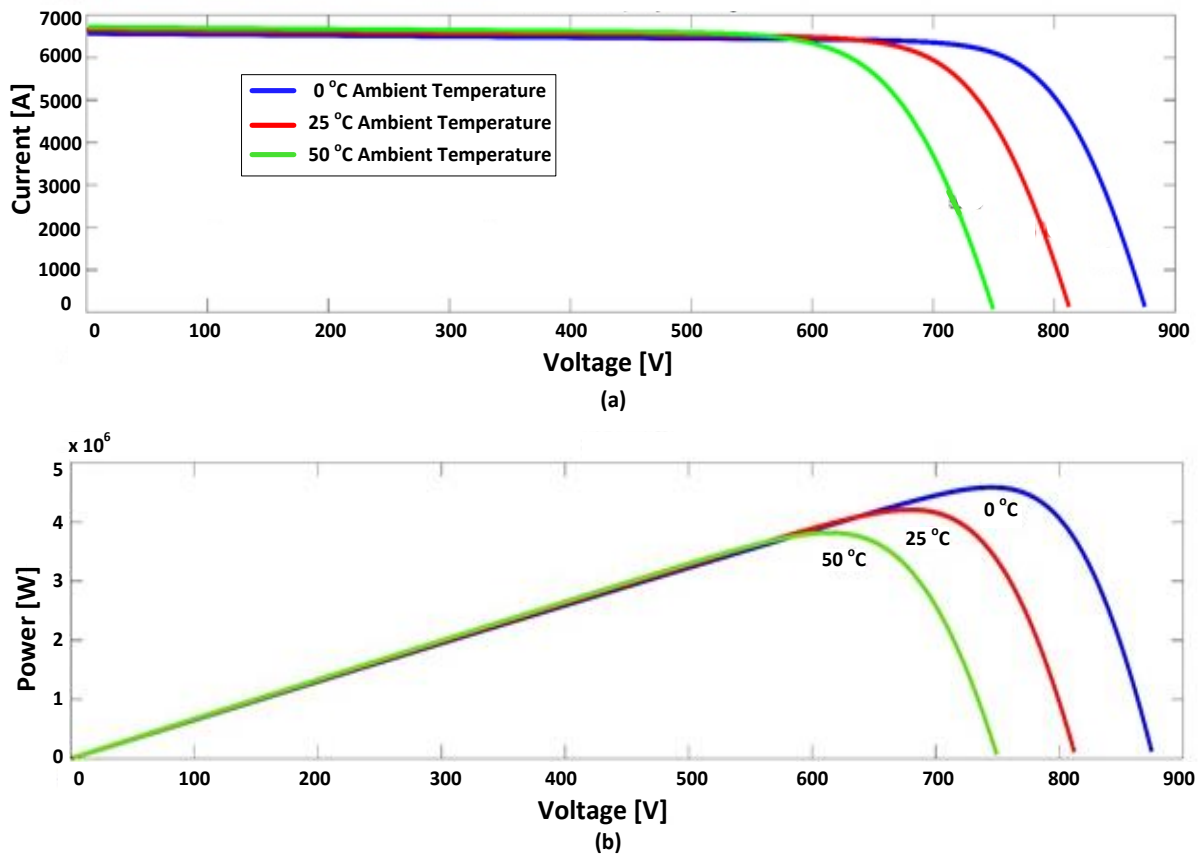| Parameter	Designation	Rating
Peak rated power	P_{mpp} [W]	480
Cell per module	N_{cell}	96
Maximum power voltage	V_{mpp} [V]	52.26
Maximum power current	I_{mpp} [A]	9.24
Temperature coefficient of V_{oc}	$\%/C^o$	-0.31
Temperature coefficient of I_{oc}	$\%/C^o$	0.045

(a)

(b)

Fig. 4. a) I-V; b) P-V characteristics of the PV module

The equivalent circuit model defines the I-V curves of a PV cell for given operating conditions. Different models have been used depending upon the accuracy and computation. The simplest model is the single diode model of PV cell shown in Fig. 5 that have five parameters. Eqs. (1) and (2) for this model can be formulated using Kirchhoff's law as:

$$I = I_L - I_D - I_{sh} \tag{1}$$

$$I = I_L - I_o(e^{\frac{V+IR_s}{nV_T}} - 1) - \frac{V+IR_s}{R_{sh}} \tag{2}$$

where I_L is light generated current, I_o is the diode saturation current, V_T is the thermal voltage, R_s and R_{sh} represent the series and shunt resistances, respectively, and the diode ideality factor is denoted by n.
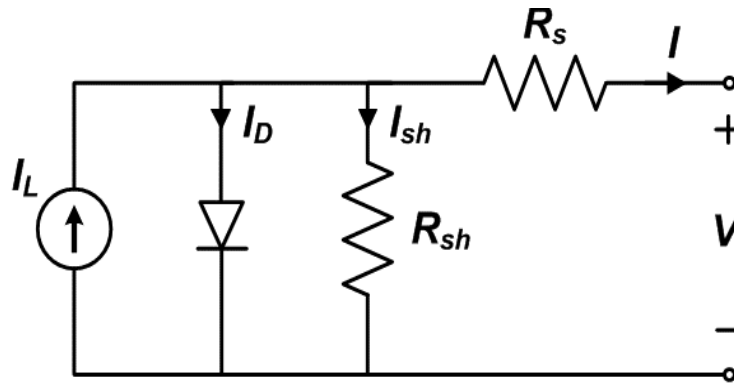
Fig. 5. Single diode model of the PV cell.

2.2. Maximum Power Point Tracking

As the solar energy is dependent on irradiance, the shape of I-V characteristics changes - as observed from Fig. 6 – making the curve non-linear. The power taken from the PV module depends upon the operating point on the curve. The maximum power output of a PV system is only available at one point which is called maximum power point (MPP). If the load resistance changes, MPP will change and the PV output power/efficiency will decrease. Therefore, we use a maximum power point tracker (MPPT) to keeps the impedance – that is seen by the PV module - constant at MPP.
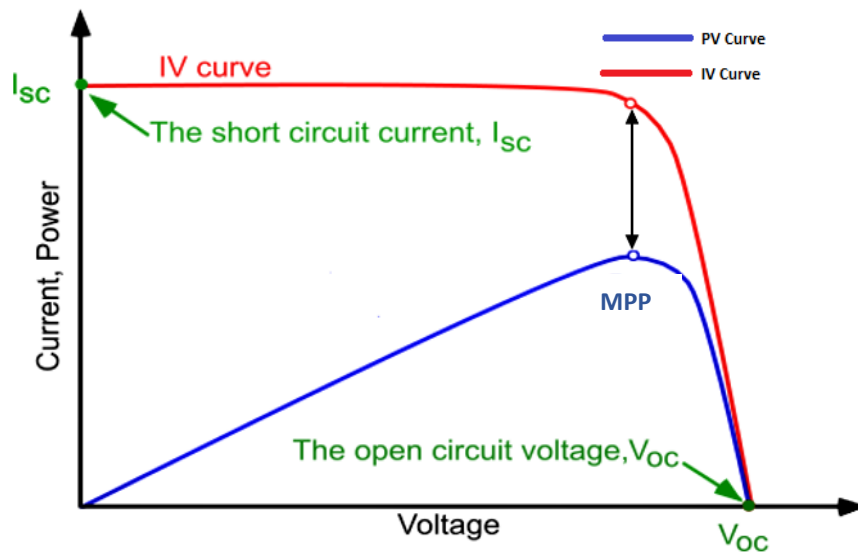

Fig. 6. MPP location on the I-V and P-V characteristics.

Different techniques have been used for tracking MPP. The most efficient technique to cope with the abrupt irradiance changes is the use of the incremental conductance (IC) method. It can be seen from the P-V characteristics, depicted in Fig. 6, that the slope of the curve is zero at MPP. IC method follows Eq. (3) principle and at MPP, dI/dV becomes equal to -I/V.

$$\frac{dP}{dV}=I\frac{dV}{dV}+V\frac{dI}{dV} \tag{3}$$

As $\frac{dP}{dV}=0$ at MPP, the final expression is:

$$\frac{dI}{dV} = -\frac{I}{V} \tag{4}$$

MPP conditions are shown in Table 2.

Table 2. MPP tracking conditions.

Condition	Constraint	Explanation
$\frac{\Delta I}{\Delta V} = -\frac{I}{V}$	If P = MPP	Achieved MPP
$\frac{\Delta I}{\Delta V} > -\frac{I}{V}$	If P < MPP	Left to MPP
$\frac{\Delta I}{\Delta V} < -\frac{I}{V}$	If P > MPP	Right to MPP

Fig. 7 shows the IC algorithm, in which firstly ΔI and ΔV is determined; then, depending upon the values, if else conditions are used for the final duty cycle. If ΔV and ΔI are both zero, then there is no change in the duty cycle. In all other cases, an increment/decrement will happen depending upon the conditions described in Table 2. If ΔI/ΔV > -I/V, an increment will occur; otherwise, decrement will take place in duty cycle.
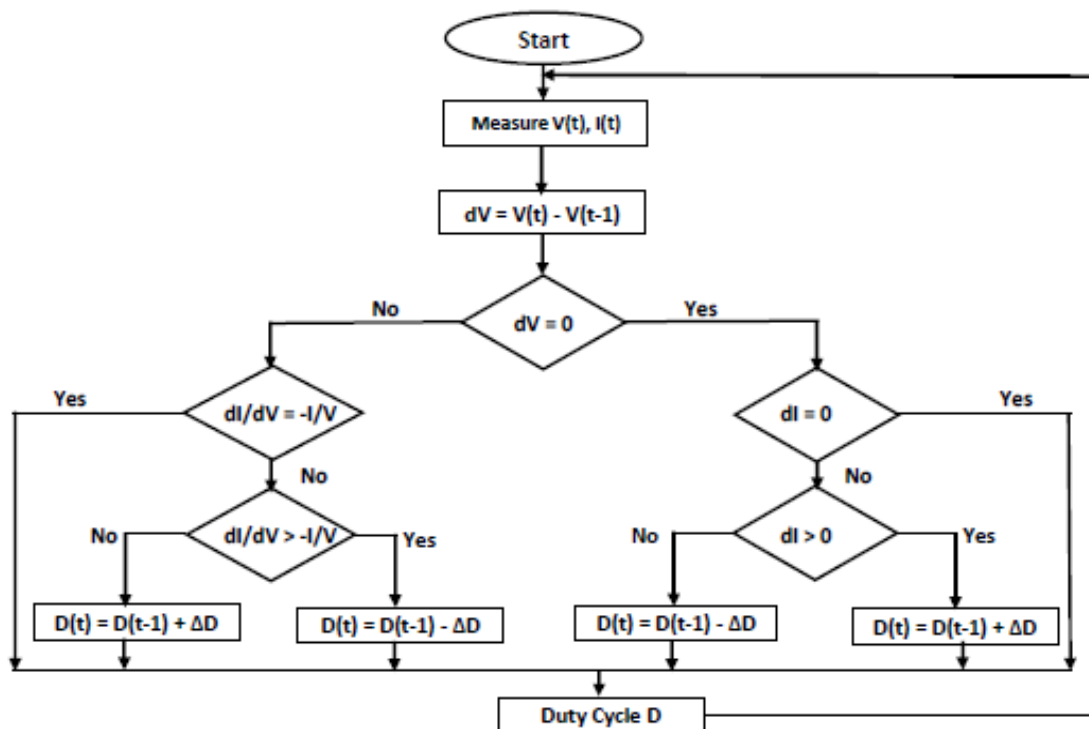

Fig. 7. Flow chart of IC.

During the calculation, the sum of I and $V \frac{dI}{dV}$ will never be exactly zero, but there will be some error. Integral regulator technique is used to eliminate this error which minimizes the residual steady-state error. It calculates the instantaneous error and adds it to the controller output after multiplying it with the controller gain.

2.3. Design of Boost Converter

A boost converter is a DC step-up transformer with high output voltage and low current compared to input voltage and current. Ideally, the total power on both sides of the converter remains constant. The output voltage is controlled with the help of switch S shown in Fig. 8, which may be MOSFET, IGBT or transistor. By controlling the duty cycle (D) of this switch, output voltage (V_o) can be controlled as:

$$V_o = \frac{-1}{1-D} \times V_i \qquad (5)$$

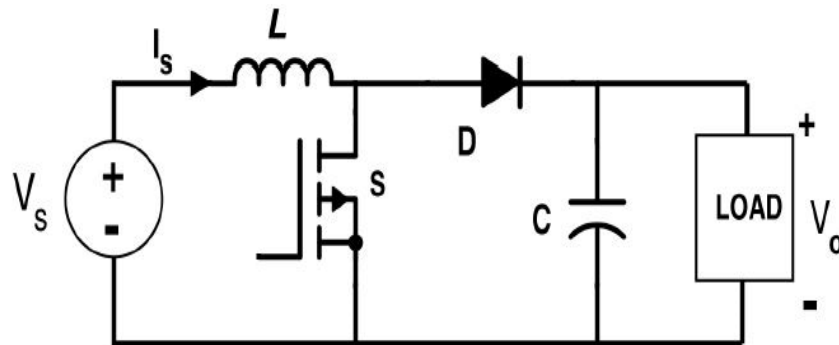$$I_L = (1-D) \times I_s \qquad (6)$$

Fig. 8. Boost converter circuit.

Eqs. (5) and (6) are used to design the converter whose duty cycle is constant along with input and output voltages; but in PV system converter - due to change in irradiance - input voltage will change, causing change to the duty cycle of the switch for operating the system on MPP. Therefore, the conventional equations for design of input inductor and capacitor are not valid here.

Input inductor and output capacitor should always operate in continuous conduction mode; both should not discharge completely during the off cycle. Therefore, the ripple in input current (ΔI_L) is usually taken as 13% of total input maximum current in Eq. (8) [19].

$$L_{boost} = \frac{V_s \times (V_o - V_s)}{\Delta I_L \times f_s \times V_o} \qquad (7)$$

Here,

$$\Delta I_L = 0.13 \times I_o \times \frac{V_o}{V_s} \qquad (8)$$

$$L_{boost} = 5.0811 \ \mu H \qquad (9)$$

The capacitor on the output side regulates the voltage and delivers the power during the half cycle of pulse. It can be calculated using Eq. (10) [20].

$$C_{boost} = \frac{P}{2 \times \omega \times u \times U_c} \qquad (10)$$

Here, U_c is the mean voltage across the capacitor, u and ω are the amplitude and angular frequency of output ripple voltage, respectively.

$$C_{boost} = 0.84215 \ mF \qquad (11)$$

The switching frequency f_s of the converter is 5 kHz because at higher frequency switching losses increase.

2.4. DC-AC Inverter

The boost converter's output is fed to the input of inverter for converting the DC power into AC power. The grid is an AC network and the inverter is being synchronized with it. There are different topologies for the designing of inverter depending upon the voltage level and harmonics requirement. Neutral point clamping (NPC) topology is selected with 3 level bridge. As shown in Fig. 9, NPC is a multilevel inverter that provides the clamping diodes for sharing proper voltage across the switches. Due to its multilevel nature, it offers good quality wave with fewer harmonics.
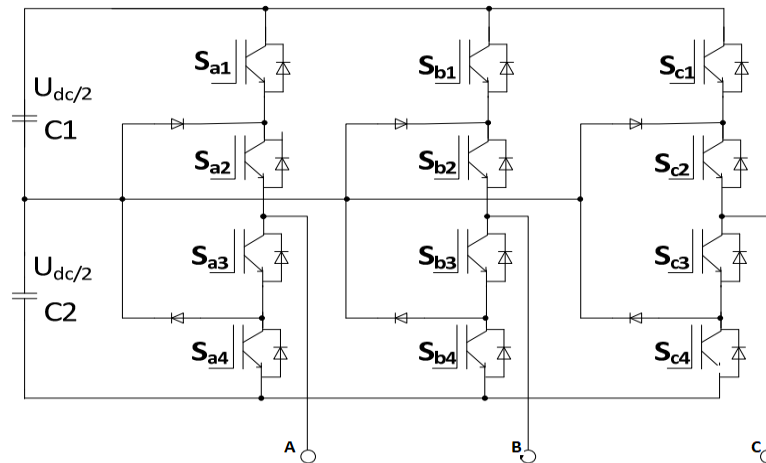
Fig. 9. NPC topology of the utilized inverter.

To control the switching frequency of the inverter, the sinusoidal pulse width modulation (SPWM) technique is used. A sine reference signal is compared with two triangular carrier signals for generating the desired pulses as shown in Fig. 10. In NPC topology, switches S_1 and S_3 operate in complementary mode, S_2 and S_4 also operate in complementary mode; otherwise, it may short circuit the source through any leg of inverter switches. The switching frequency of inverter is 1650 Hz when a 50 Hz sine wave is compared with 1650 Hz triangular wave. Fig. 11 shows NPC switching pulses pattern.
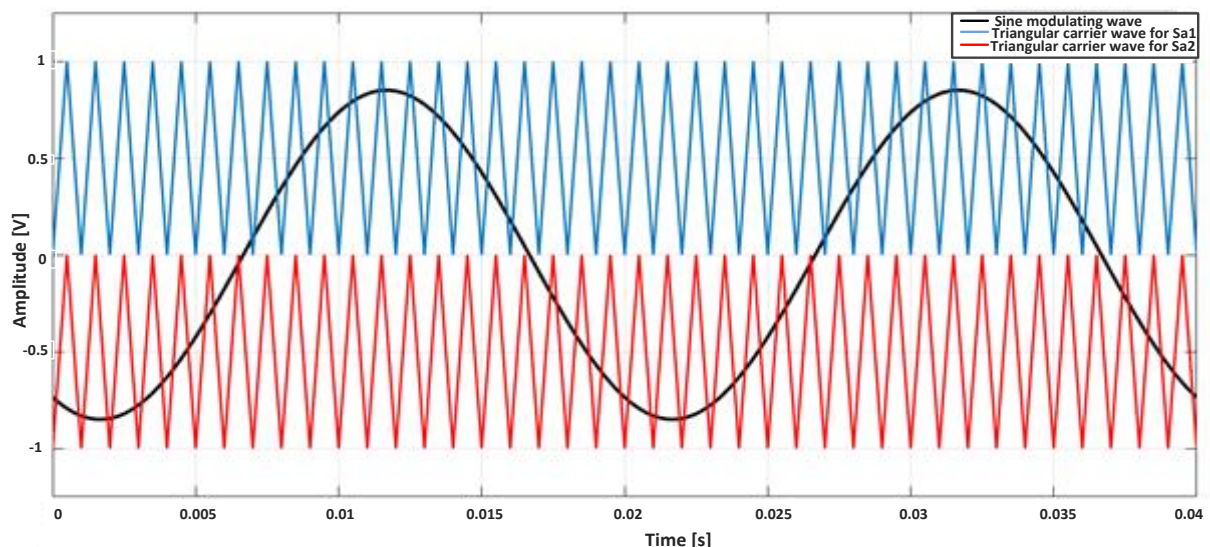
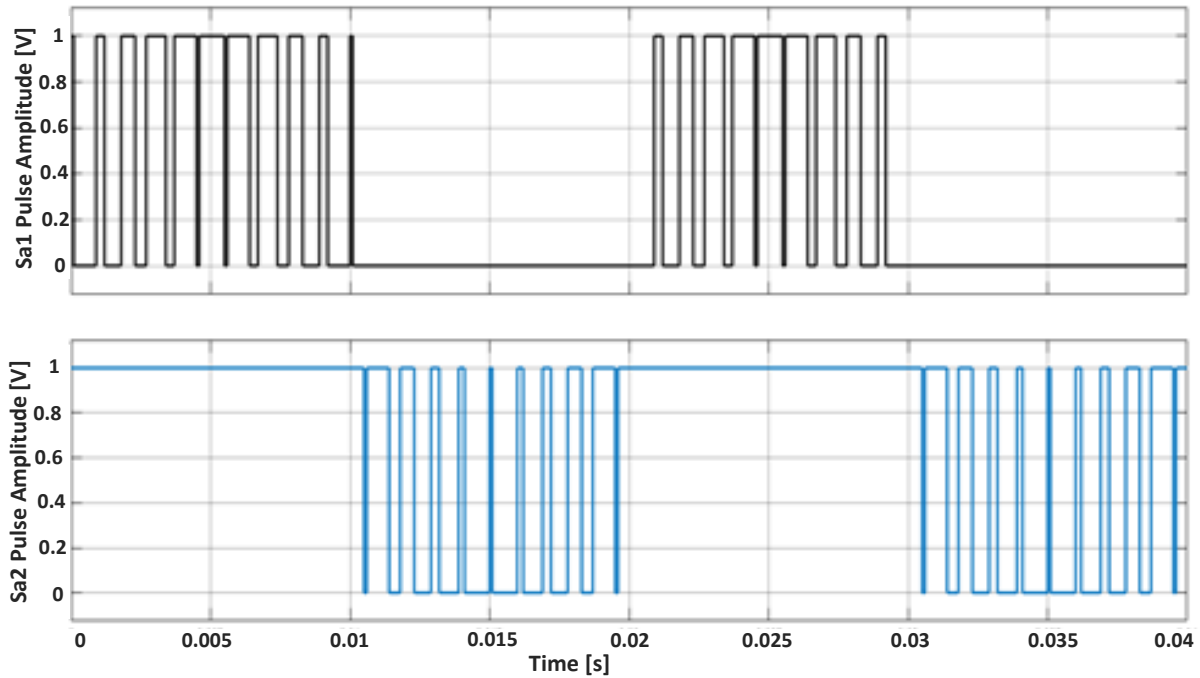Fig. 10. NPC switching modulating wave vs carrier wave.

Fig. 11. Pattern of NPC switching pulses.

2.5.   Grid Synchronization and Inverter Power Control

Grid is a source of power and can deliver or absorb any amount of power. For a grid-tied PV system, the grid also acts like a battery. For the grid-tied operation, proper synchronization and power control of the inverter are vital for a stable operation. For synchronization voltages angle, magnitude and phase should be the same; otherwise, it may disturb the stability of the power system.

To control the voltage parameters of the inverter, it is compulsory to have an idea about the grid voltage magnitude, phase and frequency. As grid quantities are AC and inverter input is DC, it is necessary to transform the grid quantities into d-q frame of reference, i.e., a 2-D synchronous frame rotating at a constant speed so that quantities in that frame appear as constant quantities. The following two equations are used for d-q transformation [21]:

$$\begin{bmatrix} V_d \\ V_q \end{bmatrix} = \sqrt{\frac{2}{3}} \begin{bmatrix} \sin\omega t & \sin(\omega t - \frac{2\pi}{3}) & \sin(\omega t + \frac{2\pi}{3}) \\ \cos\omega t & \cos(\omega t - \frac{2\pi}{3}) & \cos(\omega t + \frac{2\pi}{3}) \end{bmatrix} \times \begin{bmatrix} V_a \\ V_b \\ V_c \end{bmatrix} \tag{12}$$

$$\begin{bmatrix} I_d \\ I_q \end{bmatrix} = \sqrt{\frac{2}{3}} \begin{bmatrix} \sin\omega t & \sin(\omega t - \frac{2\pi}{3}) & \sin(\omega t + \frac{2\pi}{3}) \\ \cos\omega t & \cos(\omega t - \frac{2\pi}{3}) & \cos(\omega t + \frac{2\pi}{3}) \end{bmatrix} \times \begin{bmatrix} I_a \\ I_b \\ I_c \end{bmatrix} \tag{13}$$

Two control loops have been used to control the active and reactive power. These two loops keep the power balance on both AC and DC sides of the inverter. The outer loop is the voltage loop and the inner loop is current loop. The voltage loop keeps constant the voltage at the input of inverter DC bus. As the solar irradiance changes, it ultimately causes a change in the DC voltage of inverter input. The objective of this loop is to change the active power reference, so the power delivered to the grid changes as per solar irradiance variation.

The inner current loop takes the active and reactive power reference and regulates the current fed into the grid. In our designed model shown in Fig. 12, the reactive power reference (the quadrature axis) is set to zero. Therefore, the inverter will deliver only active power to the grid and zero reactive power.
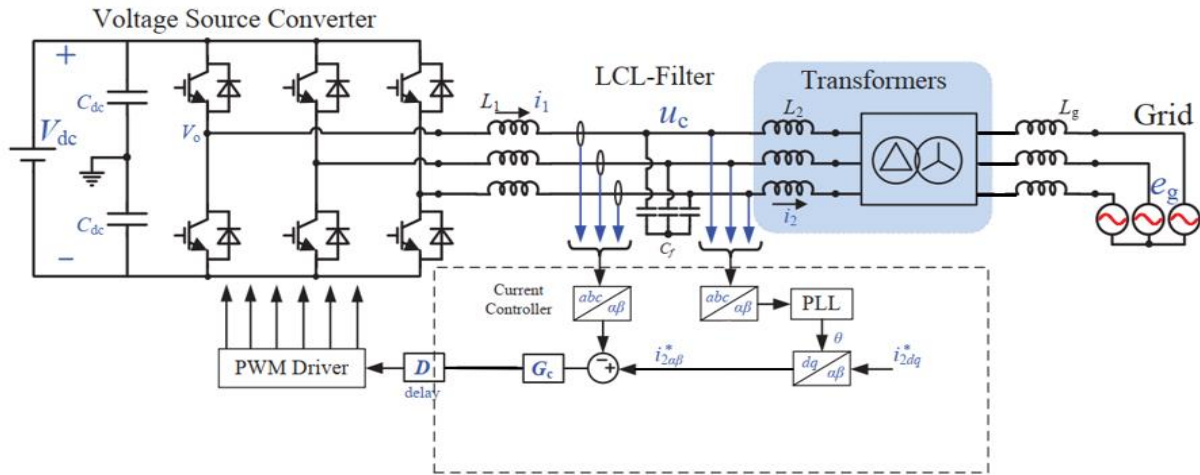

Fig. 12. Schematic configuration of the PV grid synchronization.

2.6. LCL Filter Design

Since the inverter output waveform is not a pure sinusoidal signal, it is necessary to reduce the harmonic content in that waveform. To do this, different filters can be used. However, LCL filter shown in Fig. 13 is the most suitable one, because it provides high attenuation for unwanted signals and it requires low rating inductor and capacitor.
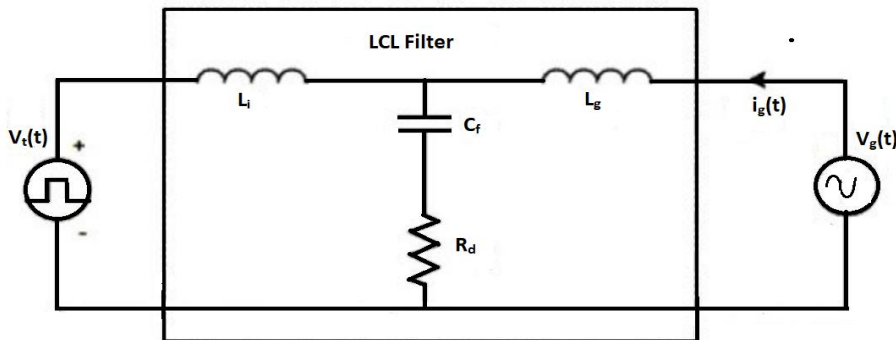

Fig. 13. LCL filter configuration.

The first step in designing LCL is to calculate the inverter side inductor (L_i), which can be done by [22]:

$$Li = \frac{U_{dc}}{16 \times f_s \times \Delta I_L} \qquad (14)$$

Here, U_{dc} is the DC link voltage, f_s is the system frequency, ΔI_L is the current ripple taken as 10% of maximum current and can be calculated as:

$$\Delta I_L = 0.1 \times \frac{P_{nominal} \times \sqrt{2}}{V} \qquad (15)$$

After putting all parameters in Eq. (14), the final value of inverter side inductor is:

$$Li= 20.94 \ \mu H \tag{16}$$

The grid side inductor L_g can be calculated as:

$$Lg= 0.6 \times Li \tag{17}$$

$$Lg= 16.766 \ \mu H \tag{18}$$

Finally, the filter capacitor (C_f) is designed in a way so that there should be a maximum 5% oscillation in the inverter output voltage for the stable operation of grid-tied PV system. The capacitance can be calculated using the below formulas as:

$$C_f= \frac{P_{nominal}}{\omega_{grid} \times V_{ph\text{-}grid}} \tag{19}$$

$$C_f=4.01146 \ mF \tag{20}$$

The final step is to have a look at the resonance frequency of the filter. At resonance frequency, impedance and admittance cancel each other and the circuit behaves as a resistor. The resonance frequency must be far from power frequency and minimum should be half the switching frequency. Resonance frequency can be determined using Eq. (21).

$$f_{res}= \frac{1}{2\Pi} \times \sqrt{\frac{Li+Lg}{Li \times Lg \times C_f}} \tag{21}$$

The resonance frequency came to be 778 Hz, and the value of damping resistor (R_d) is calculated with the help of this one. Damping resistor reduces oscillation and prevents short circuit at a resonance frequency. It can be calculated as:

$$R_d= \frac{1}{3 \times \omega_{res} \times C_f} \tag{22}$$

$$R_d= 0.01763 \ \Omega \tag{23}$$

3. MODELING OF THE DESIGNED HRES IN SIMULINK

The designed grid-tied HRES system is modeled in Simulink, which is a MATLAB blocks-based programming interface that provides the modeling, analysis and simulation of dynamic systems. For modeling HRES, Simscape blocksets are used. All modeling has been done using the calculated parameters, and the effect of real time conditions is also included in the block's parameters, i.e., transformer saturation, excitation current, inductor resistance, etc.

Firstly, in the PV system, the desired level of irradiance and temperature is achieved using the signal builder block and the output of this block acts as input of PV array block. Furthermore, the boost converter circuit is built under real conditions and switching pulses are given to the MOSFET of converter by MPPT to extract the maximum power solar modules. To convert the DC voltage to AC voltage, SPWM technique is used on the NPC converter and LCL is constructed for filtering purpose.

Fig. 14 shows the complete schematic modeling of the designed captive power plant. The calculation about the sub blocks parameters was discussed in section 3. In modeling, transformer saturation, controller limits, IGBT internal resistances, and damping resistor effects have also been considered. A PV array block is used for implementing one string of PV modules; the second string is the replica of it. The parameters given in Table 1 are inserted into this module. The output of PV the array is connected to boost converter with the help of coupling capacitor which stabilizes the dc voltage with the help of MPPT. NPC 3-level bridge inverter is used for DC/AC conversion which is connected to grid with the help of LCL filter.
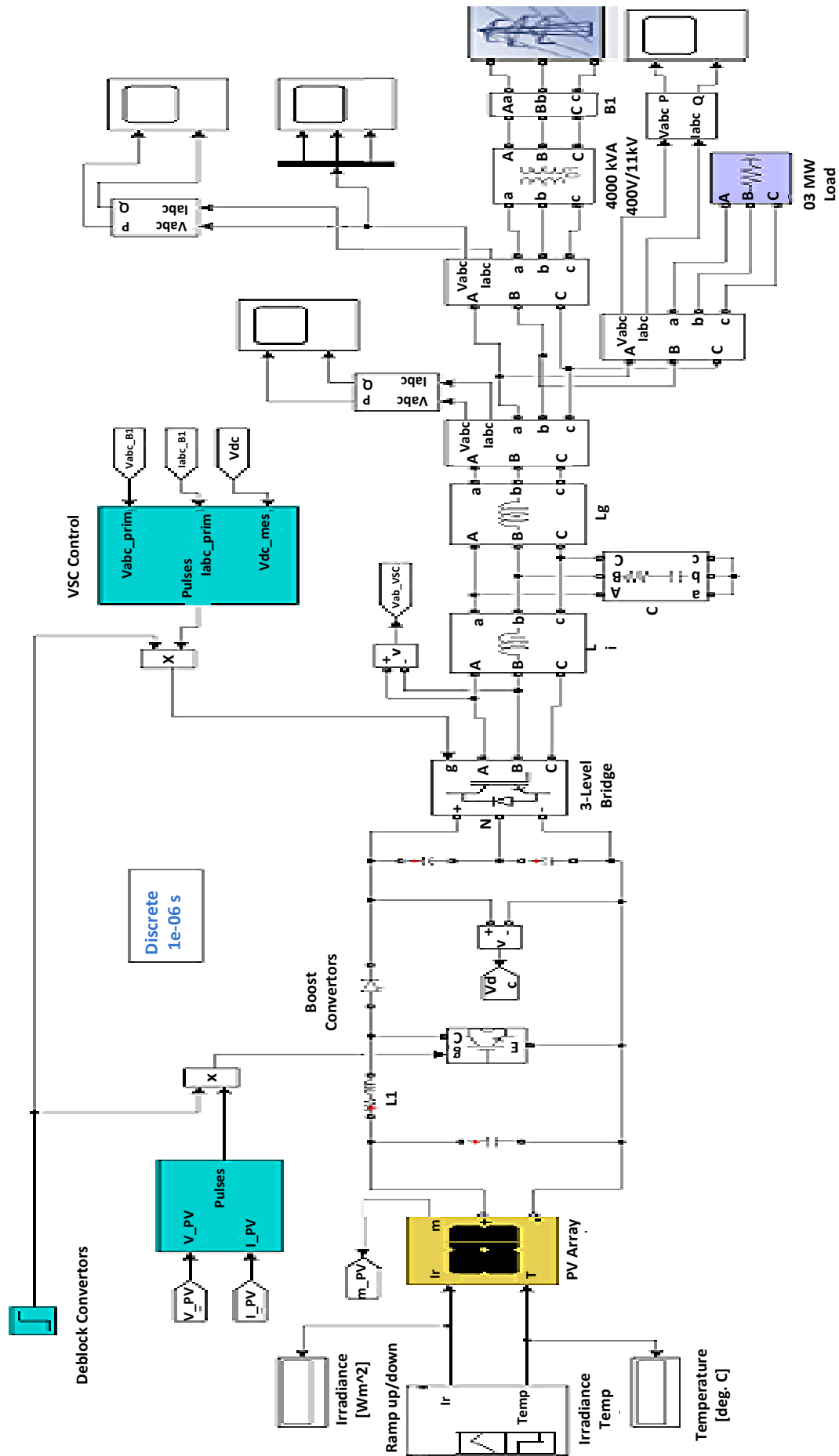
Fig. 14. Modeling of the proposed system in Simulink.

Grid is an infinite source of power because it has a slack/swing bus which can handle any amount of power. In Pakistani distribution companies, regional grid input voltage is 132 kV which is step down to 11 kV for distribution purpose and then 11 kV is further reduced to 400 V. The length of 11 kV feeder - whose inductance and resistance effect is also taken into account - for our selected consumer is 2 km. Finally, for the synchronization of both sources, the phase lock loop is used to track the angle of grid voltage used in d-q frame for generating the desired pulses and grid phase angle voltage. For observing the behavior of system, three phase power measurement block - which only considers the positive sequence component for measurement - is used.

3.1. Power Generation

PV system is the base load power plant, responsible for providing the maximum power to the system. Therefore, the frequency of the incoming PV system should be slightly more than the grid; then, it will be able to deliver the power to the grid and load. Fig. 14 shows that the point of common coupling is the node between the LCL filter and 400V/11 kV distribution transformer. At this point, the power distribution happens and due to variance in the industrial load, extra power is fed to the grid with the help of net metering. The three-phase peak voltage at point of common coupling (PCC) during the grid-tied operation is shown below in Fig. 15. In which, during the transient period when t < 1s, the voltage error is more than 5 % but after this the voltage steady state error reduces to 2% and finally the voltage becomes stable after 0.4 s.
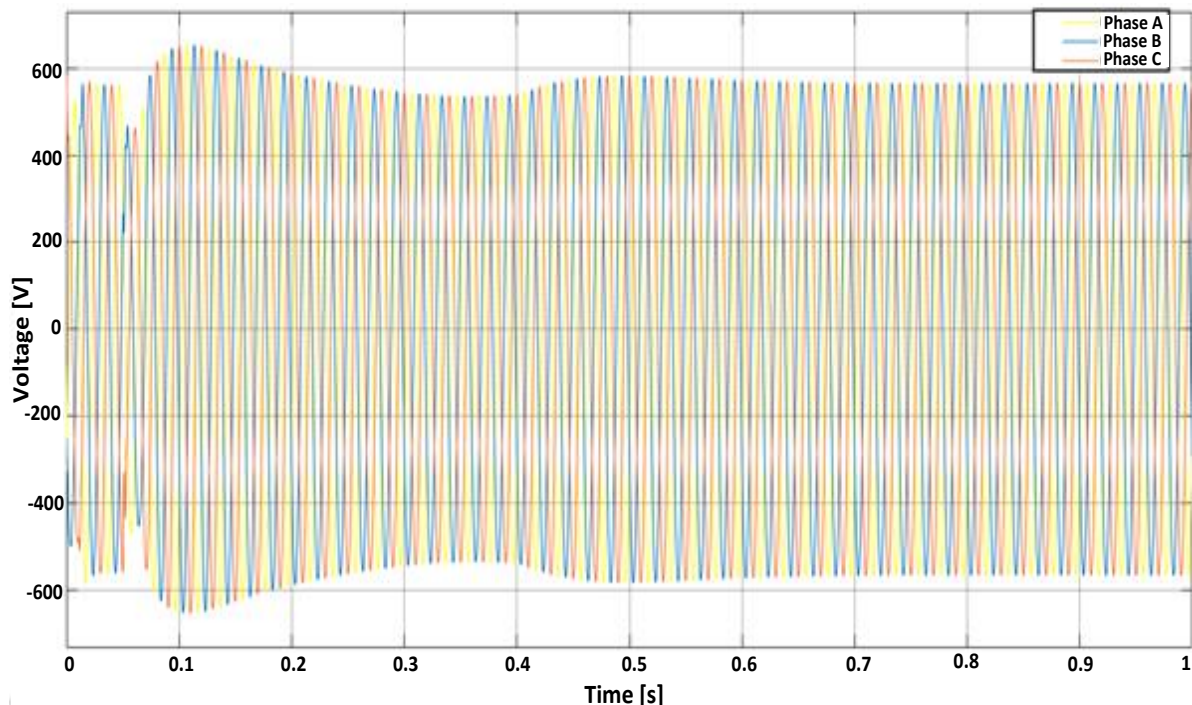

Fig. 15. Peak voltage at the 400 V bus.

3.2. Power Distribution on the 400 V Bus

Power at the common bus varies with irradiance, and during the low irradiance and night time, the power will also be delivered by the grid as per load demand but during the

high irradiance, PV system will transfer surplus power to the grid. So, an exchange of power occurs as per weather conditions and load demand as depicted in Fig. 16.

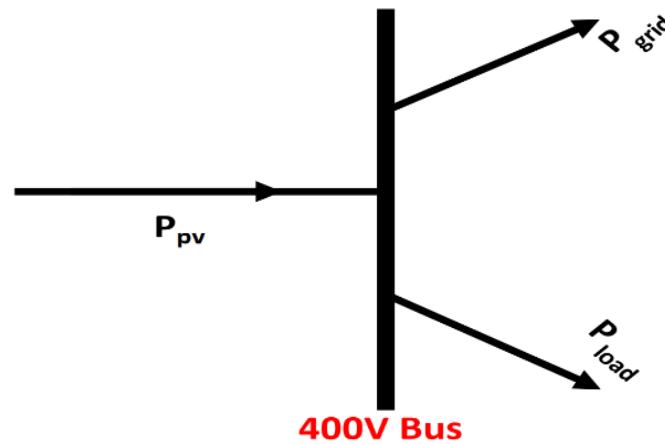$$P_{pv} = P_{load} + P_{grid} \tag{24}$$

Fig. 16. Power distribution at the 400 V bus.

P_{grid} may be the source or load of power depending upon the solar irradiance level. When delivering power to the load and act as a source, it will be negative. A complete dynamic response of the system is shown in Fig. 17 which shows that after 0.4 s, the steady state error is zero. The power delivered by the PV system is equal to the sum of the power absorbed by the grid and the load. The system transient response time can be reduced but it increases the initial percentage overshoot. Fig. 17 shows the PV system that supplies 3000 kW to the local load and additional power of the 805 kW to the grid.
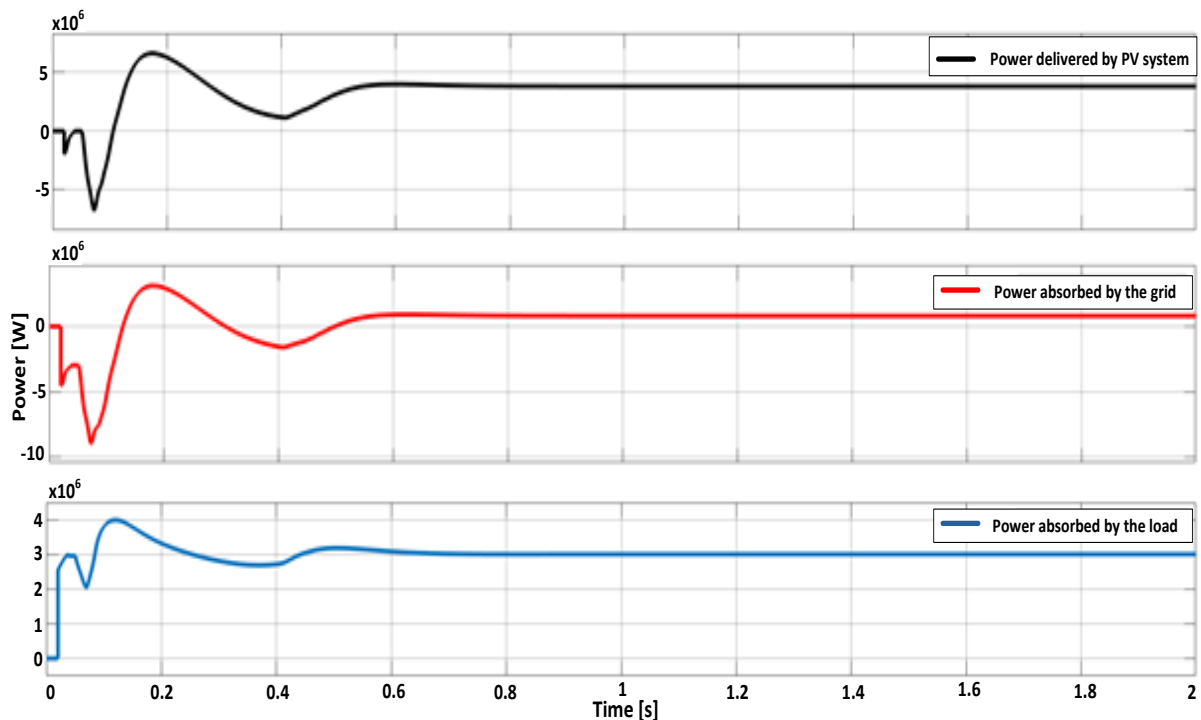
Fig. 17. Power distribution of the PV system.

3.3.   Effect of Abrupt Change in Irradiance

The intensity of irradiance on any site depends on various factors like time, weather, season and atmospheric conditions. The dust, clouds, rain and fog affect the amount of irradiance reaching the earth.

As the output power of the PV array is directly dependent upon irradiance, the system should be fast enough to overcome the response of transients. For this purpose, a step-change in irradiance is given to the PV array to study the step response which ultimately changes the output power while maintaining the grid's stability. The simulation results for the step change are shown in Fig. 18; a step change of 300 W/m² happens at 0.9 s, which shifts the irradiance at 600 W/m² and eventually causes a change in the output power of the PV array. As our load remains constant, the extra power is supplied to the grid.
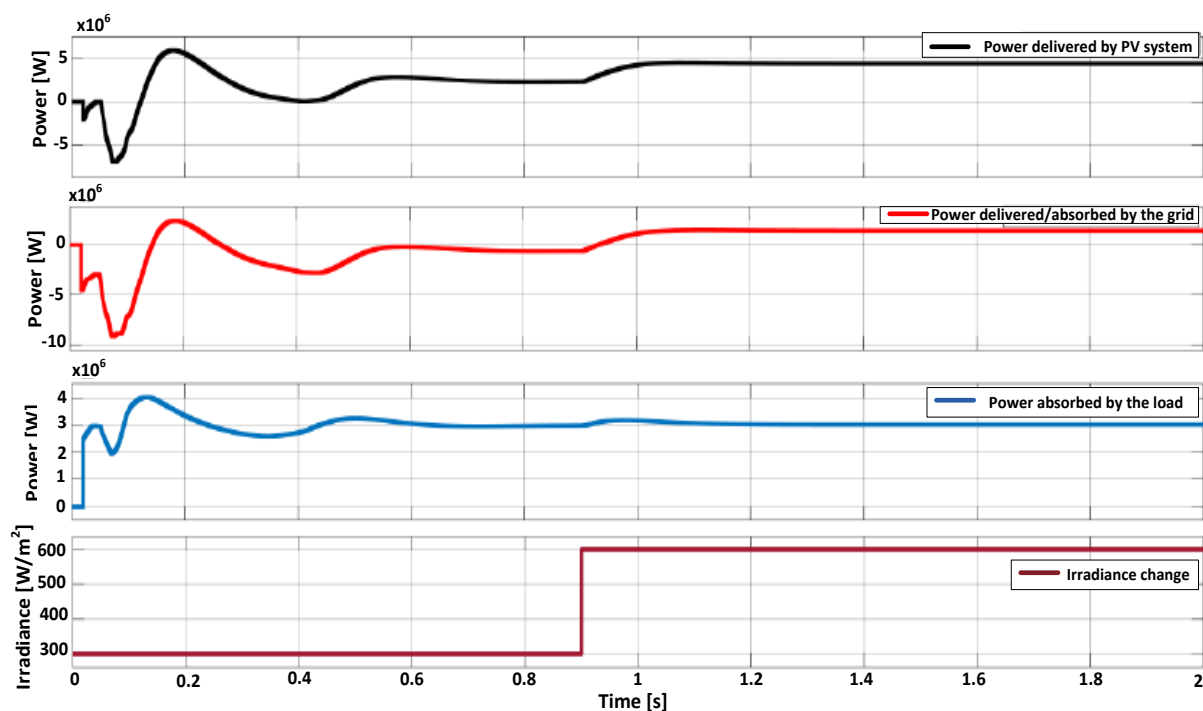

Fig. 18. HRES behavior to step change in irradiance.

3.4.   Effect of Load Variations

As the load on the power system keeps changing continuously, and the small load variations do not matter, most loads in the industry are inductive loads that run large conveyers, compressors, etc., that take large amount of current. Therefore, the system should be stable enough to bear such large disturbance, and maintain synchronization of the voltage and frequency. Therefore, a 1.5 MW abrupt change in the load has been applied at 0.9s to 1.5s for observing the system's response. It can be seen from Fig. 19 that the load increases, and the power delivered to the grid decreases, and the system remains stable.
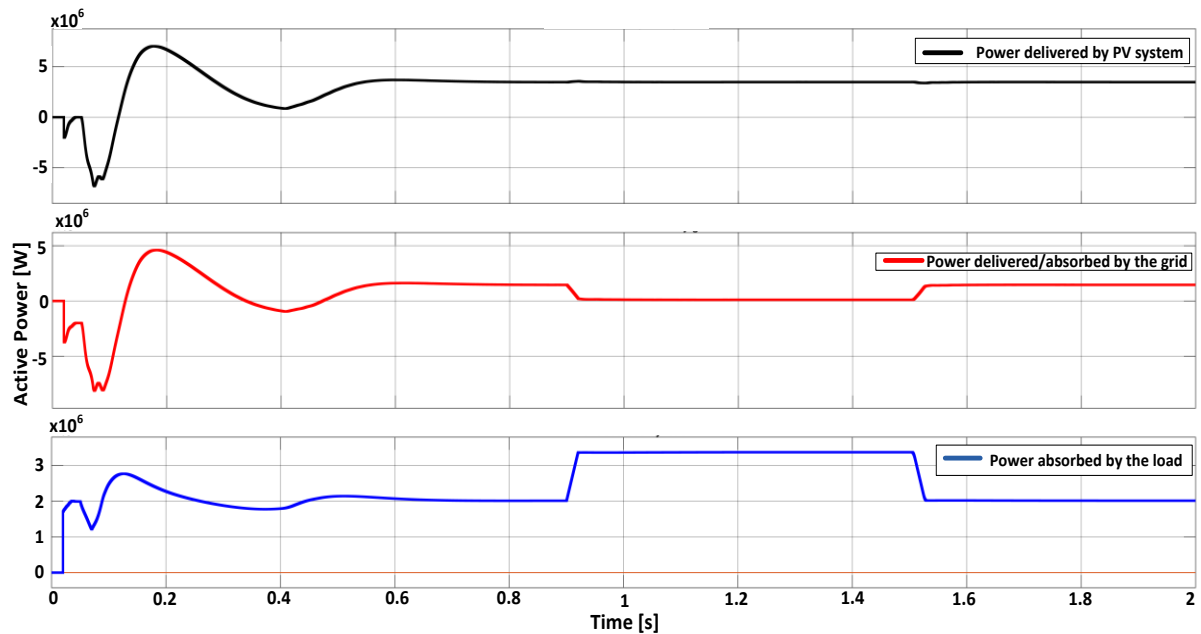
Fig. 19. Effect of load variations on the system.

4. CONCLUSIONS

A detailed sizing, modeling and dynamic analysis of a hybrid power system was presented in this paper. Firstly, the HOMER pro sizing results were depicted. They showed that the 8382 kW$_{dc}$ solar modules are required for optimum operation of the captive power plant. The dynamic analysis of the designed system was performed in Matlab/Simulink, which shows transient and steady-state behavior of the grid-tied HRES under Pakistani conditions.

For tracking the maximum power point, a modified IC method was used to improve the residual steady state error. After designing the boost converter, DC/AC NPC inverter was synchronized with the grid with the help of a phase-locked loop (PLL). An LCL filter was used between the grid and the inverter. Because of synchronization, both sources should have the same waveform. The grid is designed by 132 kV slack bus for extra power handling. The voltage, frequency and power factor were the main parameters of designed system for smooth operation. The voltage on the 400 V bus remained under 400±5% and the frequency remained 50±2% designed limit which improved the system's stability. The current quadrature component was set to zero which stabilized the system's power factor at unity. The system behavior under disturbance and the irradiance step response were presented. They showed that the HRES power was fed to the grid while maintaining the voltage and frequency within the limit. The following primary result and conclusions have been deducted during testing of the designed HRES:

- The system provided lowest per unit cost of energy that amounts to 0.1025 $/kWh.
- Designed HRES could handle load fluctuations of 1.5 MW.
- The system had fast enough response to tackle 300 W/m² step change in irradiance by increasing the power delivered to grid.
- Voltage of the designed HRES remained stable at 400V during any interruption in the system.

The paper finds limitations and hurdles in easing the renewable energy integration and suggested the system design to the industrial units in Pakistan. Finally, simulation results show that the designed system can handle interrupts and disturbances. The IC control, inverter active and reactive power control used, had fast response which improved the stability of whole system. This system sizing and modeling show that the deigned system if implemented can greatly reduce site energy cost while maintaining the same power quality.

In future, the designed system can be improved by reducing the settling time and percentage overshoot of the system.

REFERENCES

[1] International Energy Agency, *Energy Access Outlook 2017: From Poverty to Prosperity*, International Energy Agency: Paris, France, 2017.

[2] A. Khan, S. Chowdhury, "GHG emission reduction and global warming adaptation initiatives by UNFCCC," *2nd International Conference on the Developments in Renewable Energy Technology*, pp. 1-6, 2012.

[3] A. Omer, "Energy, environment and sustainable development," *Renewable and Sustainable Energy Reviews*, vol. 12, no. 9, pp. 2265–2300, 2008.

[4] I. Nassar, I. Elsayed, M. Abdella, "Optimization and stability analysis of offshore hybrid renewable energy systems," *2019 21st International Middle East Power Systems Conference,* pp. 583-588, 2019.

[5] M. Jayakumar, V. Rajini, "Investigation of photovoltaic water pumping system," *2013 International Conference on Circuits, Power and Computing Technologies*, pp. 275-282, 2013.

[6] V. Raviprasad, R. Singh, "Optimal sizing of PV power plant using sizing ratio for powering critical load with parallel redundant architecture," *IET Chennai Fourth International Conference on Sustainable Energy and Intelligent Systems*, pp. 101-107, 2013.

[7] S. Das, T. Malakar, "A probabilistic load flow with uncertain load using point estimate method," *2018 15th IEEE India Council International Conference,* pp. 1-5, 2018.

[8] F. Huneke, J. Henkel, J. González, G. Erdmann, "Optimisation of hybrid off-grid energy systems by linear programming," *Energy, Sustainability and Society*, vol. 2, no. 1, pp. 1-19, 2012.

[9] A. Asrari, A. Ghasemi, M. Javidi, "Economic evaluation of hybrid renewable energy systems for rural electrification in Iran—A case study," *Renewable and Sustainable Energy Reviews*, vol. 16, no. 5, pp. 3123-3130, 2012.

[10] N. Tahir, H. Jatala, "Design optimization and analysis of hybrid power system," *2014 International Conference on Energy Systems and Policies*, pp. 1-5, 2014.

[11] M. Nurunnabi, N. Roy, "Grid connected hybrid power system design using HOMER," *2015 International Conference on Advances in Electrical Engineering*, pp. 18-21, 2015.

[12] M. Chaichan, A. Kazem, M. El-Din, A. Al-Kabi, A. Al-Mamari, H. Kazem, "Optimum design and evaluation of solar water pumping system for rural areas," *International Journal of Renewable Energy Research*, vol. 7, no. 1, pp. 12-20, 2017.

[13] F. Mosbah, T. Iqbal, "Sizing of a large isolated solar energy system for Bani Walid, Libya," *Journal of Clean Energy Technologies*, vol. 6, no. 6, pp. 385-393, 2018.

[14] R. Elavarasan, G. Shafiullah, N. Kumar, S. Padmanaban, "A state-of-the-art review on the drive of renewables in Gujarat, state of India: present situation, barriers and future initiatives," *Energies*, vol. 13, no. 1, pp. 40, 2019.

[15] P. Benalcazar, A. Suski, J. Kamiński, "Optimal sizing and scheduling of hybrid energy systems: the cases of Morona Santiago and the Galapagos Islands," *Energies,* vol. 13, no. 15, pp. 3933, 2020.

[16] M. Al Mehedi, M. Iqbal, "Optimal design, dynamic modeling and analysis of a hybrid power system for a catamarans boat in Bangladesh," *European Journal of Electrical Engineering and Computer Science*, vol. 5, no. 1, pp. 48-61, 2021.

[17] Y. Abid, M. Khan, T. Muhammad, "Design and analysis of hybrid power generation system for rural electrification. a case study," *2019 3rd International Conference on Energy Conservation and Efficiency,* pp. 1-6, 2019.

[18] L. Ahsan, M. Iqbal, "Design of an optimal hybrid energy system for a captive power plant in Pakistan," *2021 IEEE 12th Annual Information Technology, Electronics and Mobile Communication Conference*, pp. 0820-0826, 2021.

[19] H. Massawe, *Grid Connected Photovoltaic Systems with SmartGrid Functionality*, Master Thesis, Institutt for elkraftteknikk, Trondheim, Norway, 2013.

[20] F. Gao, D. Li, P. Loh, Y. Tang, P. Wang, "Indirect dc-link voltage control of two-stage single-phase PV inverter," *2009 IEEE Energy Conversion Congress and Exposition,* pp. 1166-1172, 2009.

[21] D. Hameed, S. Hamayoon, A. Malik, O. Ansari, "Solar grid-tied inverter, with battery back-up, for efficient solar energy harvesting," *2016 IEEE Smart Energy Grid Engineering*, pp. 95-99, 2016.

[22] H. Li, W. Wu, M. Huang, H. Chung, M. Liserre, F. Blaabjerg, "Design of PWM-SMC controller using linearized model for grid-connected inverter with LCL filter," *IEEE Transactions on Power Electronics,* vol. 35, no. 12, pp. 12773-12786, 2020.